ACS Chemical Neuroscience

Letter

Cite This: ACS Chem. Neurosci. 2019, 10, 3419−3426

pubs.acs.org/chemneuro

Calbindin-D28K Limits Dopamine Release in Ventral but Not Dorsal Striatum by Regulating Ca^{2+} Availability and Dopamine Transporter Function

Katherine R. Brimblecombe,*[,†,‡] Stefania Vietti-Michelina,[†] Nicola J. Platt,[†] Rahel Kastli,[†] Ahmad Hnieno,[†] Caitlin J. Gracie,[†] and Stephanie J. Cragg*[,†,‡]

[†]Department of Physiology, Anatomy and Genetics, University of Oxford, Oxford OX1 3PT, United Kingdom

[‡]Oxford Parkinson's Disease Centre, University of Oxford, Oxford OX1 3PT, United Kingdom

Supporting Information

ABSTRACT: The calcium-binding protein calbindin-D28K, or calb1, is expressed at higher levels by dopamine (DA) neurons originating in the ventral tegmental area (VTA) than in the adjacent substantia nigra pars compacta (SNc). Calb1 has received attention for a potential role in neuroprotection in Parkinson's disease. The underlying physiological roles for calb1 are incompletely understood. We used cre-loxP technology to knock down calb1 in mouse DA neurons to test whether calb1 governs axonal release of DA in the striatum, detected using fast-scan cyclic voltammetry ex vivo. In the ventral but not dorsal striatum, calb1 knockdown elevated DA release and modified the spatiotemporal coupling of Ca^{2+} entry to DA release. Furthermore, calb1 knockdown enhanced DA uptake but attenuated the impact of DA transporter (DAT) inhibition by cocaine on underlying DA release. These data reveal that calb1 acts through a range of mechanisms underpinning both DA release and uptake to limit DA transmission in the ventral but not dorsal striatum.

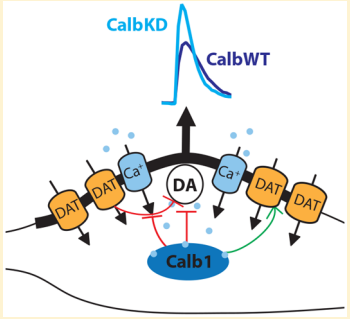

KEYWORDS: *Dopamine, calbindin-D28K, dopamine transporter, Parkinson's disease, fast-scan cyclic voltammetry*

The substantia nigra pars compacta (SNc) and ventral tegmental area (VTA) comprise a contiguous but molecularly heterogeneous collection of dopaminergic neurons that innervate the striatum in a topographic pattern, innervating predominantly the dorsal and ventral striatum, respectively.[1,2] These DA neurons show heterogeneity in their expression levels of mRNA or protein for a diverse range of molecules that include D2 receptors, DA transporter (DAT), and calcium-binding protein calbindin-D28k (calb1).[1,3−7] Calb1 is expressed in VTA DA neurons at ∼2−3-fold higher levels than in SNc[3,5,7,8] and is a fast, high affinity, and mobile buffer.[9−11] The function of calb1 in DA neurons has not been well-defined, but calb1 has been of long-standing interest as a marker of preserved DA neurons in Parkinson's disease.[12,13]

In other neuron types, calb1 impacts on Ca^{2+}-dependent transmitter release, affects voltage-gated Ca^{2+} channels (VGCCs),[14,15] and regulates spatial segregation of Ca^{2+} signals by acting as both a Ca^{2+} sink and a source on unbinding or saturation.[16−18] Calb1 has been reported to limit Ca^{2+}-dependent release probability of vesicles in cultured dissociated rat VTA-enriched DA neurons.[19] Mature DA axons in situ show heterogeneity in the Ca^{2+}- and VGCC-dependence of DA transmission between the dorsal striatum (dorsal caudate-putamen, CPu) and ventral striatum (nucleus accumbens, NAc).[20] There is also a difference between regions in the spatiotemporal coupling between Ca^{2+} entry and DA release with evidence suggesting that an additional fast buffer appears to regulate this coupling in NAc.[20] Since calb1 is expressed at higher levels by DA neurons that innervate NAc than those that innervate CPu, calb1 function might be a key contributor to this divergent Ca^{2+}-dependence.

Here, we utilized a cre-loxP approach to knock down calb1 from DA neurons selectively to address whether calb1 regulates axonal DA release in dorsal or ventral striatum, and whether it impacts on different Ca^{2+}-dependence and spatiotemporal coupling. We also explored the additional impact of calb1 on how the DAT can gate DA uptake and release.

RESULTS AND DISCUSSION

Targeted knockdown of calbindin-D28k (calb1) in DA neurons was achieved by crossing homozygous floxed $Calb_{tm2}$ mice[21] with homozygous $Slc6a3^{tm1.1(cre)Bkmn}/J$ (DAT-Cre) mice,[22] creating double heterozygous mice (named CalbKD) (Supporting Information Figure S1). Heterozygous DAT-Cre mice with wild-type calb1 levels were also generated and named CalbWT to reflect the preserved Calb gene and to indicate the main point of divergence in our two key mice genotypes. A heterozygous DAT-Cre background was common to CalbKD and CalbWT mice throughout. DAT-Cre mice (CalbWT) were used as controls since there are ∼17% lower levels of DAT in heterozygous DAT-Cre

Received: June 10, 2019
Accepted: July 30, 2019
Published: July 30, 2019

DOI: 10.1021/acschemneuro.9b00325
ACS Chem. Neurosci. 2019, 10, 3419−3426

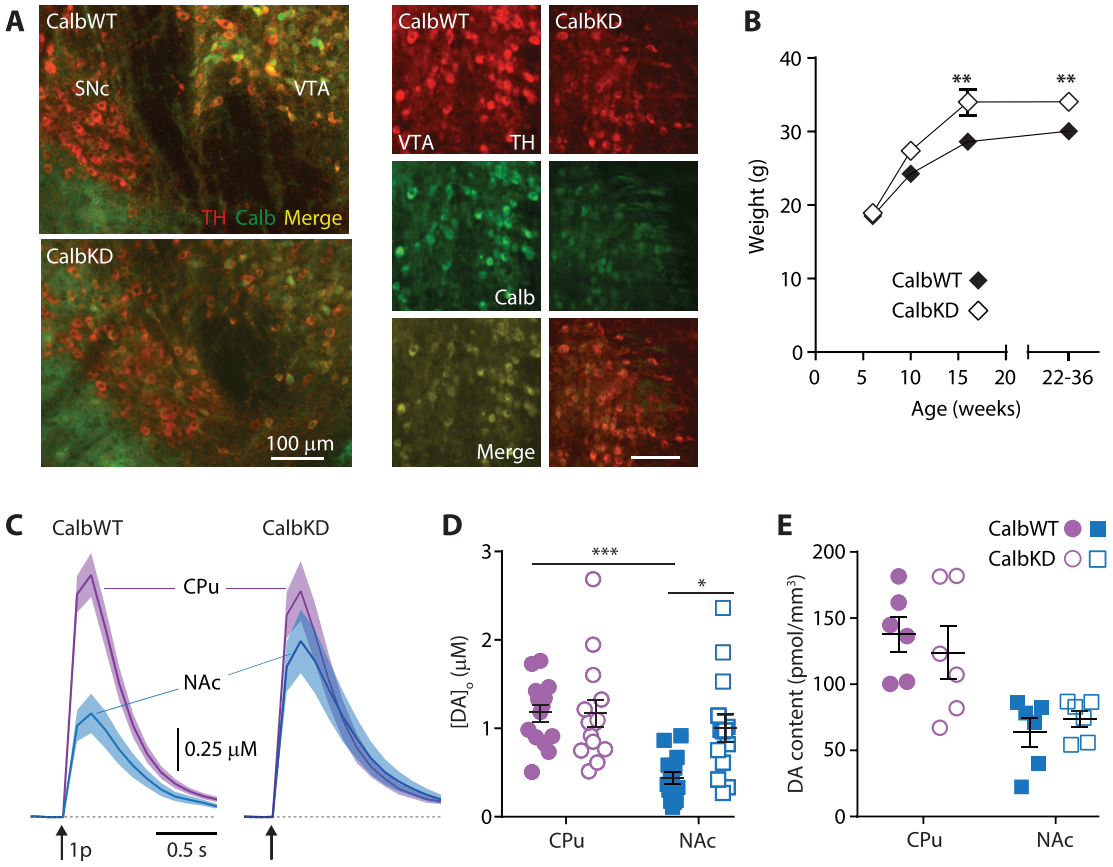

Figure 1. Calb1 knockdown leads to elevated $[DA]_o$ in NAc but not CPu. (A) Fluorescence images of midbrain showing immunoreactivity to calb1 (green), TH-positive (red), and merged (yellow). Left: Note DA cells lacking calb1 in ventral SNc, and TH- and calb1-positive cells in lateral VTA in CalbWT (upper) and to a lesser degree in CalbKD (lower); scale bar 100 μm. Right: Note decreased calb1 fluorescence in TH-positive neurons in medial VTA of CalbKD relative to CalbWT mice. (B) Mean mouse weight ± SEM vs age. Two-way ANOVA, age × genotype interaction, $F_{3,40}$ = 1.4, P = 0.26; effect of genotype: $F_{1,40}$ = 16.2, P = 0.0002, n = 5 male mice per genotype tracked from 6 to 16 weeks, n = 11 male mice at time point of culling in weeks 22−36. (C) Mean $[DA]_o$ ± SEM (shaded) vs time evoked by single pulses (arrow) in CPu (purple) and NAc (blue) in CalbWT (left) and CalbKD (right). (D) Peak $[DA]_o$ ± SEM in CPu (circles) and NAc (squares) and mean $[DA]_o$ ± SEM (black lines) for CalbWT (filled) and CalbKD (unfilled). Two-way ANOVA region × genotype, interaction $F_{1,52}$ = 5.0, P = 0.03; region: $F_{1,52}$ = 13.5, P = 0.001; genotype, $F_{1,52}$ = 5.11, P = 0.03; NAc, Sidak's posthoc t test, t_{52} = 3.18, P < 0.05; CPu, Sidak's posthoc t test, t_{52} = 0.02, P > 0.05 n = 14 sites from 5 pairs of mice. (E) DA content (pmol/mm^3) measured by HPLC-ECD from CPu (circles) and NAc (squares) of CalbWT (filled) and CalbKD (unfilled), and mean data ± SEM (black lines). Two-way ANOVA, genotype effect: $F_{1,20}$ = 0.02, P = 0.88, n = 6 samples, 3 pairs of mice. FCV data were collected in the presence of nAChR blockade (DHβE 1 μM). *P < 0.05, **P < 0.01, ***P < 0.001.

compared to true wild-type mice[22] and consequently slightly prolonged time courses for uptake for DA transients, although there is no net change in peak extracellular concentration of DA ($[DA]_o$) detected in our data set (Figure S2). In CalbKD mice, calb1-immunoreactivity was decreased in tyrosine hydroxylase (TH)-positive neurons within the midbrain, particularly within VTA (Figure 1A). CalbKD showed no gross behavioral phenotype on inspection in the home cage, but became ∼10% heavier than CalbWT mice in adulthood (Figure 1B).

We assessed whether knockdown of calb1 in DA neurons modified DA release in NAc and CPu in *ex vivo* striatal slices. Single pulses of electrical stimulation results in dual DA release events separated by just a few milliseconds, the first event arising from direct depolarization of dopaminergic axons, and a second from activation of nAChRs on DA axons by ACh released from cholinergic interneurons.[23] This artificially concurrent activation of nAChRs has very dominant effects on the short-term dynamics and characteristics of DA release.[24,25] To probe the roles of calb1 in DA axons without confounding effects of co-activation of cholinergic interneurons, we inhibited nAChRs in this study using antagonist DHβE (1 μM). Peak $[DA]_o$ evoked by single electrical stimulus pulses (in the presence of DHβE) in NAc of CalbKD mice were approximately double those seen in CalbWT controls, but were not modified in CPu (Figure 1C,D), indicating that calb1 limits DA release in NAc but not CPu. For reference, we also found that peak $[DA]_o$ was greater in NAc of CalbKD relative to CalbWT mice in drug-free conditions when nAChRs are active (Figure S3), but nonetheless DHβE was used for all other experiments reported here. We did not find any difference in DA content between genotypes in NAc, or CPu (Figure 1E), indicating that, in NAc, calb1 affects DA release but not storage. This ability of calb1 to strongly limit DA release in NAc is consistent with the ability of calb1 to rapidly bind Ca^{2+} and with previously published data in VTA-enriched cultured neurons.[19]

We tested whether calb1 knockdown modified the Ca^{2+}-dependence of DA release. In CPu, consistent with the lack of effect of calb1 knockdown on evoked $[DA]_o$, there was no difference in the relationship between $[Ca^{2+}]_o$ (range 0.6−4.8 mM) and evoked $[DA]_o$ in CalbKD vs CalbWT mice (Figure

DOI: 10.1021/acschemneuro.9b00325
ACS Chem. Neurosci. 2019, 10, 3419−3426

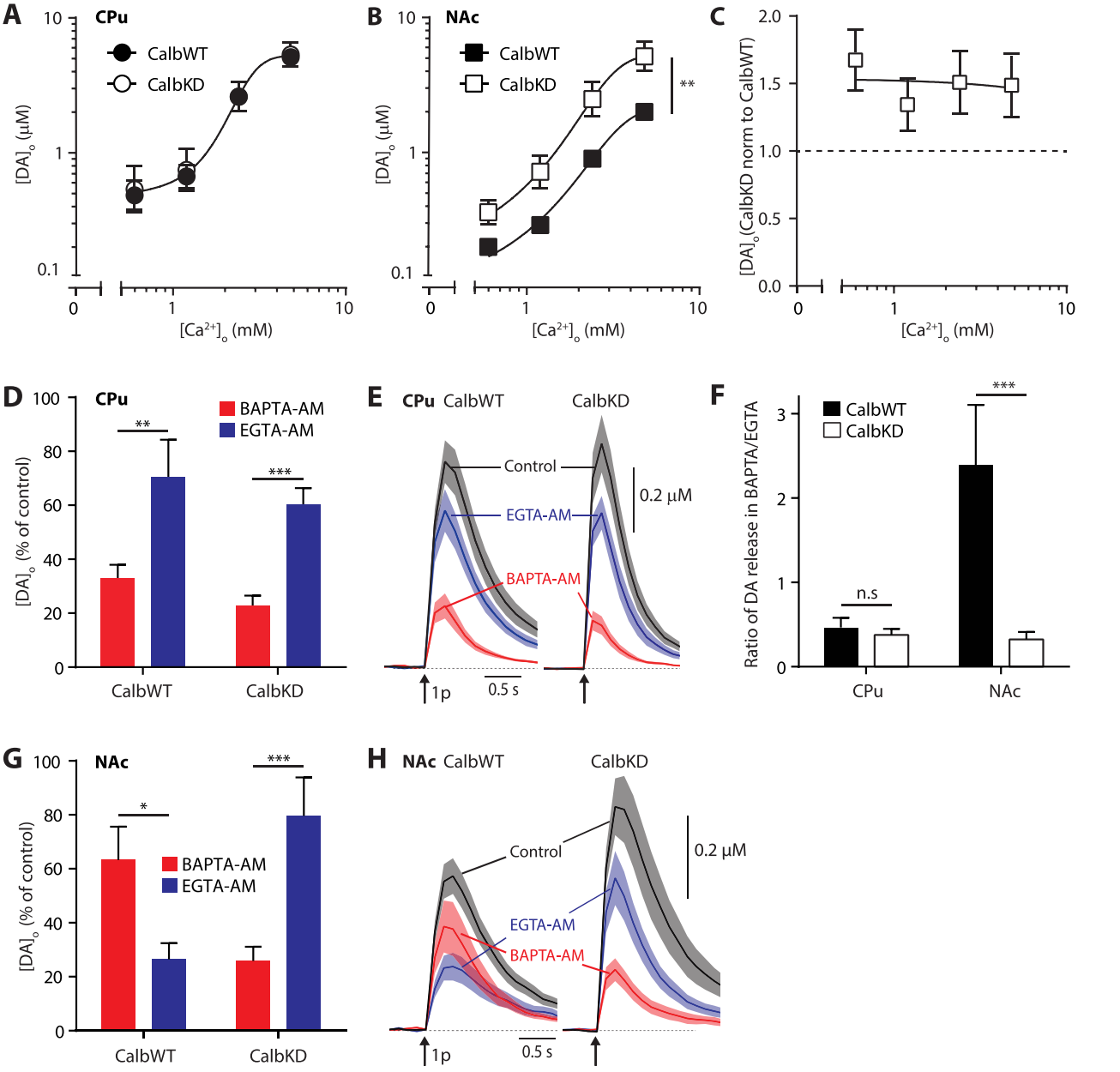

Figure 2. Modified relationship between $Ca^{2+}$and $[DA]_o$ in NAc after calb1 knockdown. (A,B) Variable slope sigmoidal curve fit of log–log transformed data of mean peak $[DA]_o$ ± SEM evoked by 1p versus $[Ca^{2+}]_o$ in CPu: (A) one curve fits both genotypes, $F_{4,32} = 0.04$, $P = 0.99$, n =. 4 Hill slope: 3.4. R^2 CPu: 0.81. NAc: (B) curves significantly different between genotypes, $F_{4,24} = 6.2$, $P = 0.0014$. R^2 NAc 0.93 (calbWT) and 0.82 (calbKD). No change in Hill slope: CalbKD 2.9 vs CalbWT 2.5,$F_{1,24} = 0.4$ $P = 0.84$, $n = 4$ experiments/animals. CalbWT (filled) and CalbKD (unfilled). (C) Peak evoked $[DA]_o$ in CalbKD expressed normalized to value in CalbWT at each $[Ca^{2+}]_o$ used, linear regression not different from zero slope, $P = 0.83$. $N = 4$ pairs of animals. (D,G) Peak $[DA]_o$ (% of control) ± SEM in the presence of BAPTA-AM (100 μM) (red) or EGTA-AM (100 μM) (blue) in CPu (D) or NAC (G). In CPu: two-way ANOVA: genotype × chelator interaction, $F_{1,51} = 1 \times 10^{-4}$, $P = 0.99$; genotype effect, $F_{1,51} = 1.60$, $P = 0.21$. In NAc: two-way ANOVA: genotype × chelator interaction, $F_{1,48} = 18.9$, $P < 0.0001$. (F) Ratio of DA release in BAPTA-AM:EGTA-AM (±SEM) in CPu and NAc in CalbWT (filled) and CalbKD (unfilled). Two-way ANOVA: genotype × region interaction, $F_{1,50} = 9.2$, $P = 0.004$. (E,H) $[DA]_o$ ± SEM (shaded) vs time in response to single pulses (1p, arrow) in CalbWT (left) and CalbKD (right) in control conditions (black) and BAPTA-AM (red) or EGTA-AM (blue) conditions, in CPu(E) and NAc (H). DHβE (1 μM) present throughout. *$P < 0.05$, **$P < 0.01$, ***$P < 0.001$ Sidak's post-test following two-way ANOVA. $N = 4$ pairs of animals, 14 sites/genotype/region.

2A). However, in NAc, evoked $[DA]_o$ was significantly greater at all $[Ca^{2+}]_o$ (Figure 2B) but with no change in apparent cooperativity (Hill slope: CalbKD 2.9 vs CalbWT 2.5 P = 0.84). $[DA]_o$ in CalbKD was consistently ~1.5-fold that seen in CalbWT across the range of $[Ca^{2+}]_o$ used (Figure 2C). Thus, calb1 in DA axons in NAc appears to function to reduce net intracellular $[Ca^{2+}]$. The relationship between stimulation frequency and DA release (either in the presence or absence of nAChR-blockade) was not modified by calb1 knockdown (Figure S4) consistent with the weak impact of $[Ca^{2+}]_o$ on the frequency response for DA release.[26] The impact of D_2 autoreceptor activation on DA release was also not modified (Figure S5).

DOI: 10.1021/acschemneuro.9b00325
ACS Chem. Neurosci. 2019, 10, 3419–3426

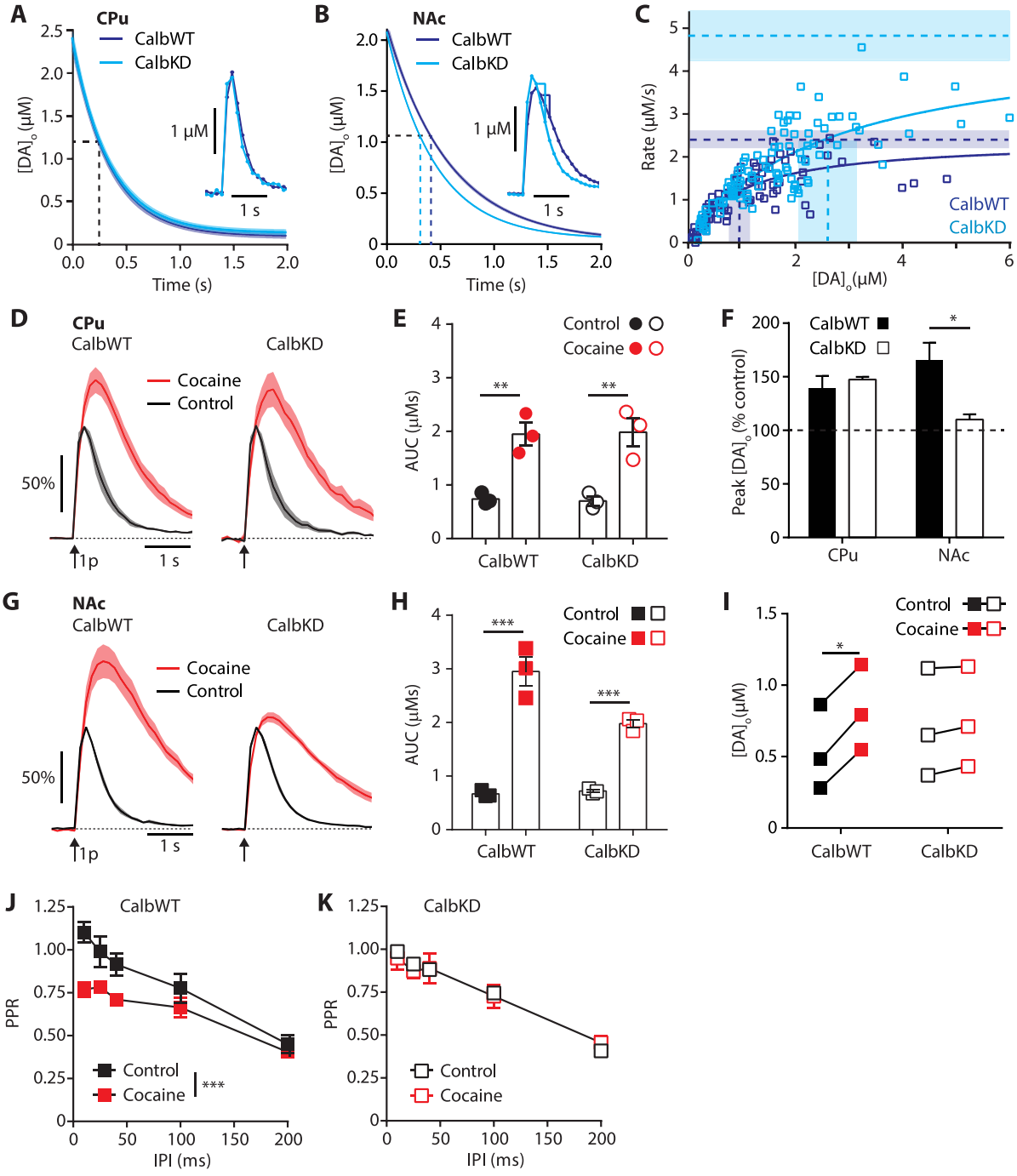

Figure 3. Calb1 knockdown modifies DA uptake kinetics and DAT regulation of DA release in NAc. (A,B) One-phase exponential decay curve fits (±95% confidence intervals, shaded) for falling phases of mean $[DA]_o$ transients versus time that were concentration-matched, evoked by single pulses in CalbWT (dark blue) and CalbKD (light blue) in CPu (A) and NAc (B). CPu, comparison of k, $F_{1,422} = 0.1$, $P = 0.76$. NAc, comparison of k, $F_{1,350} = 64.9$, $P < 0.0001$, $n = 9$ from 3 mice. Dashed lines show $t_{1/2}$. Insets show typical full $[DA]_o$ profiles and indicate points in NAc of sampling decay rates shown in C. (C) Maximum decay rates seen for each transient versus $[DA]_o$ at that rate for CalbWT (dark blue) and CalbKD (light blue). Unconstrained Michaelis–Menten curve fits (solid lines), V_{max} and K_m are indicated in dashed horizontal and vertical lines respectively ± SEM (shaded). Comparison of fits, $P = 0.0032$, $n = 73$ transients per genotype. (D,G) $[DA]_o$ ± SEM (shaded) vs time in response to single pulses (1p, arrow) in CalbWT (left) and CalbKD (right) in control conditions (black), and cocaine (5 μM, red), in CPu (D) and NAc (G) of CalbWT and CalbKD mice. Data are normalized to predrug controls conditions, scale bar indicates 50% of control. (E,H) Area under the curve (AUC) ± SEM of DA transients seen in control (black) and cocaine (red) in CalbWT (filled) and CalbKD (unfilled) for CPu (E) of NAc (H). CPu: Two-way ANOVA: no drug × genotype interaction, $F_{1,8} = 0.04$, $P = 0.84$; effect of genotype $F_{1,8} = 7 \times 10^{-6}$, $P = 1.0$. NAc: Two-way ANOVA: drug × genotype interaction, $F_{1,8} = 13.3$, $P = 0.007$; effect of genotype $F_{1,8} = 10.7$, $P = 0.01$. (F) Peak evoked $[DA]_o$ ± SEM in the presence of cocaine expressed as % of control conditions. Two-way ANOVA: genotype × region interaction, $F_{1,8} = 9.1$, $P = 0.017$; Sidak's post-test: CalbWT vs CalbKD, CPU, $t_8 = 0.56$, $P > 0.05$, NAc, $t_8 = 3.7$, $P < 0.05$. (I) Peak evoked $[DA]_o$ (μM) paired before and after cocaine ± SEM for individual experiments in CPu and NAc of CalbWT and CalbKD. Two-way ANOVA with repeated measures: cocaine × genotype interaction, $F_{1,4} = 124.6$, $P = 0.0004$, Sidak's post-tests: control vs cocaine, CalbWT, $t_4 = 18.8$, $P < 0.001$, CalbKD, $t_4 = 3.0$, $P > 0.05$, $n = 3$ experiments, 3 animals. (J,K) Paired-pulse ratios (PPR) for $[DA]_o$ detected in response to a second pulse expressed as a fraction of $[DA]_o$ detected by a single pulse, versus

DOI: 10.1021/acschemneuro.9b00325
ACS Chem. Neurosci. 2019, 10, 3419−3426

Figure 3. continued

interpulse interval (IPI) in NAc in control conditions (black) and in cocaine (red) for CalbWT (J) and CalbKD (K). In CalbWT: Two-way ANOVA effect of cocaine: $F_{1,20} = 25.0$, $P < 0.0001$. In CalbKD: $F_{1,20} = 0.05$, $P = 0.82$, $n = 3$ sites from 3 animals. DHβE (1 μM) present throughout. *$P < 0.05$, **$P < 0.01$, ***$P < 0.001$, main effect of drug or Sidak's post-tests following two-way ANOVA.

Calb1 in other neuron types can bind Ca^{2+} to restrict its availability, but it can also be a source of Ca^{2+} upon unloading or saturation, generating zones of enhanced Ca^{2+} availability.[17,27] Calb1 might therefore affect the spatiotemporal availability of Ca^{2+} in an interrelated manner, through which changing the temporal availability of Ca^{2+} can cause spatial diffusion distance to be modified.[11] To explore the impact of calb1 on the spatiotemporal coupling of Ca^{2+} to DA release, we used the intracellular exogenous Ca^{2+} chelators EGTA-AM and BAPTA-AM that, through slow and fast kinetics, respectively, reflect whether coupling is relatively slow/loose or fast/tight. We have previously shown that, in CPu, Ca^{2+} entry in wild-type mice is relatively loosely coupled to DA release, following significant effects of EGTA-AM and BAPTA-AM.[20] n CPu in CalbWT and CalbKD mice, we find that EGTA-AM and BAPTA-AM decreased evoked $[DA]_o$ to, respectively, 60−70% and 20−30% of control conditions in both genotypes (Figure 2D−F), indicating that calb1 does not govern spatiotemporal coupling of Ca^{2+} to DA release in CPu. In NAc, we have previously shown in wild-type mice that EGTA-AM paradoxically decreases DA release to a greater extent than BAPTA-AM.[20] One candidate explanation is that BAPTA-AM is potentially facilitating DA release, for example, by limiting a fast source of Ca^{2+} that is negatively coupled to DA release. In NAc of CalbWT mice, as in wild-type mice, we find that EGTA-AM decreased evoked $[DA]_o$ to ∼30% of control conditions whereas BAPTA-AM decreased evoked $[DA]_o$ to ∼60% of control. Conversely, in CalbKD mice, EGTA-AM and BAPTA-AM decreased evoked $[DA]_o$ to, respectively, ∼70% and ∼30% of control (Figure 2F−H). The ratio of effects of BAPTA vs EGTA on DA release are therefore inverted in CalbKD vs CalbWT in NAc (Figure 2F). These data indicate that calb1 participates in the spatiotemporal coupling of Ca^{2+} entry to DA release in NAc, and support a hypothesis that calb1 provides a fast inhibitory source of Ca^{2+} that limits DA release in NAc.[20]

The DA transporter (DAT) plays a variety of roles in governing DA transmission. In addition to removing extracellular DA by uptake and regulating extracellular summation, DATs also limit underlying DA release via apparently inhibiting mobilization of the vesicle pool in a manner that is limited or offset by Ca^{2+}. In other neurons, Ca^{2+} regulates levels of release and the relationship to short-term plasticity[28,29] and also maintains pools of readily releasable vesicles.[30−33] At striatal release sites for DA, DATs also appear to contribute to these processes, limiting initial release levels, short-term plasticity, and availability of DA vesicles for release in a Ca^{2+} dependent manner.[26,34−37] DAT inhibitors such as cocaine not only prolong the extracellular lifetime of DA but also promote DA release when $[Ca^{2+}]_o$ is low.[34,35] It has been proposed that these actions of DAT inhibitors on uptake and vesicle mobilization are dissociable and reflect distinct functions of DATs.[26,36] Given the apparent role for calb1 in determining intracellular Ca^{2+} availability in NAc, we hypothesized that calb1 knockdown might modify the ability of DATs to limit underlying release.

We first examined whether there were changes to DA uptake kinetics via the DAT. In CPu, the falling phases of extracellular DA transients were similar between CalbKD and CalbWT mice (Figure 3A), but in NAc, DA transients decayed at a faster rate in CalbKD than in CalbWT mice ($k = 2.6 \pm 0.04$ vs 1.7 ± 0.05 s^{-1}, exponential approximations) with a correspondingly shorter mean half-life (0.31 vs 0.40 s) (Figure 3B). For NAc, we constructed Michaelis−Menten-type plots of maximum decay rate for each transient versus $[DA]_o$ at that rate and found a higher V_{max} and apparent K_m in CalbKD compared to CalbWT (Figure 3C, CalbWT: V_{max} 3.9 ± 0.46 μM s^{-1}, K_m 2.0 ± 0.4 μM, $R^2 = 0.88$; CalbKD: V_{max} 7.1 ± 1.2 μM s^{-1}, K_m 4.2 ± 1.1 μM, $R^2 = 0.77$). These data indicate enhanced DA uptake rates in the NAc of CalbKD relative to CalbWT mice, suggesting that calb1 limits DA uptake via DATs. Differences in DA uptake rates have previously been reported between CPu and NAc, and are assumed to be due to greater DAT levels in CPu than NAc.[38] However, our data show that calb1 appears to limit the DA uptake rate in NAc, which could also contribute to the lower rates seen in ventral vs dorsal striatum. The elevated K_m seen in CalbKD mice also suggests that calb1 modifies how DATs bind DA. The mechanism responsible is not defined but might include an increase in monomeric/oligomeric ratio which impacts on K_m and V_{max}.[39,40] High DA concentrations have been shown to dissociate DAT oligomers,[41] which is an important mechanism in developing tolerance in cocaine addiction.[42]

We then tested whether calb1 knockdown modified how DATs regulate underlying DA release, by exploring the impact of DAT inhibition by cocaine (5 μM) on peak $[DA]_o$ evoked by single pulses. We were mindful of two potentially opposing outcomes. On the one hand, because DAT inhibitors potentiate peak $[DA]_o$ to the greatest extent in lower $[Ca^{2+}]_o$ conditions,[35] we hypothesized that the hyper-$[Ca^{2+}]$ condition resulting from calb1 knockdown might lead to a reduced effect of DAT inhibition on peak $[DA]_o$. However, on the other hand, since DA uptake rates are greater in NAc of CalbKD mice, a DAT inhibitor might conversely have an enhanced effect on peak $[DA]_o$. In CPu, cocaine profoundly extended the decay phases and areas under the curve of $[DA]_o$ transients (Figure 3D−F) and increased peak $[DA]_o$ compared to drug-free controls to the same extent in both genotypes (Figure 3F). In NAc, however, cocaine profoundly extended the decay phases and areas under the curve of $[DA]_o$ transients in both genotypes (Figure 3G,H) but only increased peak $[DA]_o$ in CalbWT and not CalbKD (Figure 3F,G,I). This attenuated effect of cocaine on peak $[DA]_o$ in CalbKD vs CalbWT mice was seen across a range of cocaine concentrations (0.5−5 μM) (Figure S6). The range of $[DA]_o$ seen in controls in these data sets were similar in both genotypes (Figure 3I) to account for cocaine being a competitive antagonist. The attenuated ability of cocaine to increase peak $[DA]_o$ in NAc suggests that either the pool of vesicles that cocaine mobilizes has already been mobilized for release by calb1 knockdown, or that calb1 is required for DAT to inhibit mobilization of the release pool. Consistent with an interaction between how calb1 and DATs limit DA release, we

DOI: 10.1021/acschemneuro.9b00325
ACS Chem. Neurosci. 2019, 10, 3419−3426

also found an impact of calb1 knockdown on how DATs govern short-term plasticity of DA release. In NAc from CalbWT mice, cocaine reduced paired-pulse ratios (PPRs) of DA release for short interpulse intervals as seen in WT mice[26] (Figure 3J), consistent with an elevation in the initial release of DA from the releasable pool after DAT inhibition. However, in CalbKD mice, cocaine did not modify PPRs (Figure 3K). Therefore, calb1 in NAc appears overall to help limit DA uptake via DATs, but also to support the DAT in limiting release of the vesicle pool.

In summary, we have identified that calb1 in NAc limits DA release through a range of mechanisms that include reducing intracellular Ca^{2+} availability, limiting the Ca^{2+}-dependent releasability of the vesicle pool, and promoting how DATs limit releasability of the vesicle pool. Our findings raise speculations relating to the long-known sparing of calb1-expressing VTA DA neurons in Parkinson's disease. Since our data indicate that calbKD mice have a hyper-Ca^{2+} phenotype, they support the hypothesis that calb1 helps to protect VTA DA neurons by buffering intracellular Ca^{2+}, which is likely to be protective against many of the molecular insults that contribute to parkinsonian degeneration.[43] Furthermore, the effects of calb1 on apparent DAT function could also have profound implications for PD pathology. By limiting DAT function in VTA neurons, calb1 may minimize cytosolic DA concentrations and, in turn, the formation of toxic DA metabolites.[44] Thus, neuroprotection conferred on DA neurons by calb1 might arise from both a buffering of Ca^{2+}-induced metabolic burden and also from a lowering of DAT function. Intriguingly, although calb1 has long been considered likely to exert neuroprotective effects, experiments to validate have yielded mixed outcomes.[45,46] Our data raise a cautionary note for experiments exploring neuroprotection by calb1 where toxins used to model PD are DAT substrates for example, 6-OHDA and MPTP: experimentally induced changes to calb1 levels will be mirrored by changes to DAT function that may modify the accumulation or efficacy of DAT-dependent toxins. The resolution of whether calb1 itself is neuroprotective may therefore require investigations using DAT-independent models of PD.

METHODS

Mice and Tissue Preparation. Homozygous $Calb_{TM2}$ were generated from a heterozygous $Calb_{TM2}$ breeding pair generously donated by Prof. Meyer[21] (University of Munich) (available from Jax, ID 031936 and EMMA: name B6.(R1)-Calb1tm2Mpin) (Figure S1) and crossed with homozygous $DAT^{IREScre}$ (Jax, ID 006660),[22] generating double heterozygous offspring with decreased calb1 expression in DAT-expressing cells. We chose to make heterozygous knockdown rather than homozygote deletion to minimize potential confounding adaptations that might accompany deletion of a Ca^{2+} buffer. Mice were genotyped using a PCR protocol: annealing temperature 51 °C, 34 cycles, forward primer sequence TGA CTG CCT ACC CAT CAT CC, reverse primer sequence CCT GAG CAC CGA TTA ATC AGC. For controls with wild-type levels of calb1 (CalbWT), we used age- and sex-matched heterozygous $DAT^{IREScre}$ mice to control for the impact of the DAT-Cre. Male and female mice were used throughout this study. Mice were killed by cervical dislocation, the brains were removed, and 300 μm coronal striatal slicewere s prepared in ice-cold HEPES-based buffer saturated with 95% O_2/5% CO_2, containing in mM: 120 NaCl, 20 $NaHCO_3$, 6.7 HEPES acid, 5 KCl, 3.3 HEPES salt, 2 $CaCl_2$, 2 $MgSO_4$, 1.2 KH_2PO_4, 10 glucose, as described previously.[20] Slices were incubated at room temperature for ≥1 h in HEPES-based buffer before experiments. All procedures were licensed to be carried out at the University of Oxford under the UK Animals (Scientific Procedures) Act 1986.

Fast-Scan Cyclic Voltammetry. Extracellular concentrations of DA ($[DA]_o$) evoked by local electrical stimuli were monitored from *ex vivo* acute coronal slices using fast-scan cyclic voltammetry (FCV) at carbon-fiber microelectrodes. Slices were superfused in a recording chamber with bicarbonate-buffered artificial cerebrospinal fluid (aCSF) saturated with 95%O_2/5%CO_2 at 31−33 °C, containing in mM: 124 NaCl, 26 $NaHCO_3$, 3.8 KCl, 0.8−3.6 $CaCl_2$ (as stated), 1.3 $MgSO_4$, 1.3 KH_2PO_4, 10 glucose. Evoked extracellular DA concentration ($[DA]_o$) was monitored by FCV using a Millar voltammeter (Julian Millar, Barts and the London School of Medicine and Dentistry) and single-use carbon-fiber microelectrodes (7−10 μm diameter) fabricated in-house (tip length 50−100 μm). A triangular voltage waveform (range −700 to +1300 mV vs Ag/AgCl) was applied at 800 V/s at a scan frequency of 8 Hz. Electrodes were switched out of circuit between scans. Electrodes were calibrated using 2 μM DA, prepared immediately before calibration using stock solution (2.5 mM in 0.1 M $HClO_4$ stored at 4 °C). Signals were attributed to DA due to the potentials of their characteristic oxidation (500−600 mV) and reduction (−200 mV) peaks.

DA recordings were obtained from dorsolateral quadrant of CPu, or nucleus accumbens core (NAc). DA release was evoked by a local bipolar concentric Pt/Ir electrode (25 μm diameter; FHC Inc., Bowdoin, ME) placed approximately 100 μm from the recording electrode. Stimulus pulses (200 μs duration) were given at 0.6 mA (perimaximal in drug-free conditions). Stimulations were single pulses (1p), trains of 5 pulses (5p) at 5−100 Hz, or pairs of pulses (2p) at interpulse intervals of 10−200 ms, repeated at 2.5 min intervals, with 1p stimulations occurring every third stimulation. Each stimulation type was recorded in at least triplicate in each recording site in all experimental conditions. Unlesss otherwise stated, data were obtained in the presence of the nAChR antagonist, dihydro-β-erythroidine (DHβE, 1 μM) to exclude the powerful and potential confounding modulatory effects of cholinergic interneurons on DA release.[47,48]

When comparing $[DA]_o$ in CPu and NAc between CalbWT and CalbKD (Figure 1C−E), one hemisphere containing both CPu and NAc from each genotype was placed in the recording chamber and allowed to settle while electrodes charged for >30 min. Three dorsolateral CPu sites and three NAc core sites were recorded in alternative genotypes in a random order. DHβE (1 μM) was present throughout recordings.

Drugs and Solutions. BAPTA-AM and DHβE were purchased from Ascent Scientific or Tocris UK; pluronic acid was from Life Technologies; EGTA-AM was from Millipore. All other reagents were purchased from Sigma-Aldrich. Stock solutions were made to 1000−2000× final concentrations in H_2O (DHβE and cocaine) or DMSO (EGTA-AM, BAPTA-AM, and L741,626) and stored at −20 °C. Drugs were diluted to their required concentrations in aCSF immediately prior to use. In cocaine experiments, cocaine was present for up to 1 h.

For EGTA-AM/BAPTA-AM experiments, striatal sections were bisected and each hemisphere was incubated for 30 min at room temperature in aCSF containing 2-hydroypropyl-β-cyclodextrin 70 μM (Sigma), probenecid 175 μM, (Sigma), pluronic acid 0.1% (Life Technologies), and either EGTA-AM, 100 μM (Millipore) or BAPTA-AM, 100 μM (Tocris), or DMSO (vehicle control).[20] Following preincubation, hemispheres were incubated for a further 30 min in the recording chamber prior to recording. Recordings were alternated between the EGTA-AM/BAPTA-AM-incubated versus nonincubated slice and at paired recording locations. EGTA-AM/BAPTA-AM effects sizes were obtained from peak $[DA]_o$ expressed as a percentage of control paired site, analogous to genotype comparisons.

HPLC-ECD. After recording electrically evoked DA release, tissue punches (2 × 1.2 mm for NAc and 2 × 2 mm for CPu) taken from pairs of CalbWT and CalbKD animals were put in perchloric acid solution (PCA) (200 μL, 0.1 M) and stored at −80 °C. On the day of measurement, all samples were homogenized using a hand-held sonicator and spun at 14 000*g* at 4 °C for 15 min. CPu samples were

DOI: 10.1021/acschemneuro.9b00325
ACS Chem. Neurosci. 2019, 10, 3419−3426

diluted 15× in PCA, and NAc samples were run neat and quantified against known concentration standards (100 nM) using a 4.6 × 150 mm Microsorb C18 reverse-phase column (Varian) and Decade II ECD apparatus with a glassy carbon working electrode (Antec Leyden) set at +0.7 V with respect to a Ag/AgCl reference electrode. The mobile phase contained 13% MeOH, NaH_2PO_4 (0.12 M), EDTA (0.8 mM), OSA (0.5 mM) pH 4.6.

Immunohistochemistry. Slices were fixed (PFA 4%) for at least 3 days, washed in PBS, resectioned to 40 μm, and incubated in 20% normal goat serum (NGS) (Jackson ImmunoResearch Laboratories Inc.) in 0.3% Triton-X-100 PBS (PBS-Tx) and 5% fetal bovine serum for 4 h. Sections were then incubated overnight at 4 °C in primary antibody for tyrosine hydroxylase (TH) and calb1 (1:500 sheep anti-TH (Abcam #ab113); 1:200 rabbit anti-calb1 (Cell Signaling #13176)) with 1% NGS, 1% fetal bovine serum. Sections were washed (PBS, 2× 0.3% PBS-TX) and incubated for 2 h at room temperature in secondary antibody (Alexa Fluor 594-AffiniPure donkey anti-sheep IgG (Jackson Laboratories cat# 713-585-147-JIR); Alexa Fluor 488-AffiniPure donkey anti-rabbit IgG Cat#711-545-152-JIR) in PBS-Tx, 1% NGS, and fetal bovine serum. After washes in PBS-Tx then PBS, sections were mounted on gelled slides with Vectashield (Vector laboratories). Sections were imaged using an Olympus BX41 microscope with a Q-Click cooled monochrome CCD camera (Olympus medical), 100 ms exposure. Monochrome images were converted to pseudocolored using Q-capture pro7 and optimized using histogram equalization.

Data Analysis and Statistics. Data were acquired and analyzed using Axoscope 10.5 (Molecular devices) and Excel macros written locally. Data are expressed as mean ± standard error of the mean (SEM), and n = number of animal or number of sites per region as stated. Data from each animal were obtained by averaging at least three recordings for each stimulus type and reported as peak $[DA]_o$ or normalized to mean control 1p conditions for each animal. Population means were compared using one- or two-way ANOVA with Sidak post-test where appropriate (raw data, and drug effects passed Shapiro-Wilk normality test) using GraphPad Prism. Curve fits were done using GraphPad Prism.

Analysis of comparative uptake rates between genotypes were based on falling phases of $[DA]_o$ and used two approaches as indicated. In one approach, we approximated falling phases to exponential decay and extracted half-lives ($t_{1/2}$) and uptake rate constants. Since uptake rate is dependent on $[DA]_o$, falling phases of individual transients > 2 μM peak max were matched for $[DA]_o$ by offsetting their time poststimulation and averaged and compared between genotypes. In another approach, we constructed a Michaelis−Menten type curve using all the data, forming a population of values for maximum decay rates (extracted over a duration of 0.25 s at the point of fastest $d[DA]_o/dt$) and for the $[DA]_o$ at which each rate was seen. The range of $[DA]_o$ was 0.15−2.64 μM. We extracted K_m and V_{max} values from unconstrained Michaelis−Menten curve fits. Data for comparison of uptake were collected from pairs of recordings between CalbWT and CalbKD mice, that is, the same electrode for each genotype pair.

■ ASSOCIATED CONTENT

Supporting Information

The Supporting Information is available free of charge on the ACS Publications website at DOI: 10.1021/acschemneuro.9b00325.

Additional results; genotyping strategy for calbKD and calbWT mice; comparison of WT vs CalbWT peak $[DA]_o$ and uptake rates (exponential decay curves); comparison of peak $[DA]_o$ in CalbWT vs CalbKD without nAChR antagonism; frequency response of DA release; comparison of D2-receptor control of DA release in CalbWT and calbKD; effect of cocaine 0.5-5 μM.(PDF)

■ AUTHOR INFORMATION

Corresponding Authors

*Mailing address: Department of Physiology, Anatomy and Genetics, Sherrington Building, University of Oxford, Oxford OX1 3PT, U.K. E-mail: Katherine.brimblecombe@dpag.ox.ac.uk.

*E-mail: Stephanie.cragg@dpag.ox.ac.uk.

ORCID

Katherine R. Brimblecombe: 0000-0003-0809-7292

Stephanie J. Cragg: 0000-0001-9677-2256

Author Contributions

K.R.B. and S.J.C. designed research and wrote the paper; K.R.B, S.V.-M, N.J.P., R.K, A.H., and C.J.G. performed experiments and analyzed data.

Funding

The work was funded by support from an MRC doctoral training grant (N.P.), BBSRC doctoral training program (S.V.-M.), and Parkinson's UK (J-1403).

Notes

The authors declare no competing financial interest.

■ ACKNOWLEDGMENTS

We thank Prof. Michael Meyer (University of Munich) for the gift of the floxed calbindin ($calb_{TM2}$) mouse line and Dr. Neil Blackledge (University of Oxford) for primer design.

■ REFERENCES

(1) Gerfen, C. R., Herkenham, M., and Thibault, J. (1987) The Neostriatal Mosaic: II. Patch- and Matrix-Directed Mesostriatal Dopaminergic and Non-Dopaminergic Systems. *J. Neurosci.* 7 (12), 3915−3934.

(2) Voorn, P., Vanderschuren, L. J. M. J., Groenewegen, H. J., Robbins, T. W., and Pennartz, C. M. A. (2004) Putting a Spin on the Dorsal-Ventral Divide of the Striatum. *Trends Neurosci.* 27 (8), 468−474.

(3) Chung, C. Y., Seo, H., Sonntag, K. C., Brooks, A., Lin, L., and Isacson, O. (2005) Cell Type-Specific Gene Expression of Midbrain Dopaminergic Neurons Reveals Molecules Involved in Their Vulnerability and Protection. *Hum. Mol. Genet.* 14 (13), 1709−1725.

(4) Greene, J. G. (2006) Gene Expression Profiles of Brain Dopamine Neurons and Relevance to Neuropsychiatric Disease. *J. Physiol.* 575 (Pt 2), 411−416.

(5) Poulin, J.-F., Zou, J., Drouin-Ouellet, J., Kim, K.-Y. A., Cicchetti, F., and Awatramani, R. B. (2014) Defining Midbrain Dopaminergic Neuron Diversity by Single-Cell Gene Expression Profiling. *Cell Rep.* 9 (3), 930−943.

(6) Grimm, J., Mueller, A., Hefti, F., and Rosenthal, A. (2004) Molecular Basis for Catecholaminergic Neuron Diversity. *Proc. Natl. Acad. Sci. U. S. A.* 101 (38), 13891−13896.

(7) Haber, S. N., Ryoo, H., Cox, C., and Lu, W. (1995) Subsets of Midbrain Dopaminergic Neurons in Monkeys Are Distinguished by Different Levels of MRNA for the Dopamine Transporter: Comparison with the MRNA for the D2 Receptor, Tyrosine Hydroxylase and Calbindin Immunoreactivity. *J. Comp. Neurol.* 362 (3), 400−410.

(8) Greene, J. G. J. G., Dingledine, R., and Grenamyre, J. T. (2005) Gene Expression Profiling of Rat Midbrain Dopamine Neurons: Implications for Selective Vulnerability in Parkinsonism. *Neurobiol. Dis.* 18 (1), 19−31.

(9) Nägerl, U. V., Novo, D., Mody, I., and Vergara, J. L. (2000) Binding Kinetics of Calbindin-D(28k) Determined by Flash Photolysis of Caged Ca(2+). *Biophys. J.* 79 (6), 3009−3018.

(10) Schwaller, B., Meyer, M., and Schiffmann, S. (2002) New" Functions for "Old" Proteins: The Role of the Calcium-Binding

DOI: 10.1021/acschemneuro.9b00325
ACS Chem. Neurosci. 2019, 10, 3419−3426

Proteins Calbindin D-28k, Calretinin and Parvalbumin, in Cerebellar Physiology. Studies with Knockout Mice. *Cerebellum 1* (4), 241−258.
(11) Eggermann, E., Bucurenciu, I., Goswami, S. P., and Jonas, P. (2012) Nanodomain Coupling between Ca^{2+} Channels and Sensors of Exocytosis at Fast Mammalian Synapses. *Nat. Rev. Neurosci. 13* (1), 7−21.
(12) Yamada, T., McGeer, P. L., Baimbridge, K. G., and McGeer, E. G. (1990) Relative Sparing in Parkinson's Disease of Substantia Nigra Dopamine Neurons Containing Calbindin-D_{28K}. *Brain Res. 526*, 303−307.
(13) Lavoie, B., and Parent, A. (1991) Dopaminergic Neurons Expressing Calbindin in Normal and Parkinsonian Monkeys. *NeuroReport 2* (10), 601−604.
(14) Lee, D., Obukhov, A. G., Shen, Q., Liu, Y., Dhawan, P., Nowycky, M. C., and Christakos, S. (2006) Calbindin-D28k Decreases L-Type Calcium Channel Activity and Modulates Intracellular Calcium Homeostasis in Response to K+ Depolarization in a Rat Beta Cell Line RINr1046−38. *Cell Calcium 39* (6), 475−485.
(15) Schmidt, H., Schwaller, B., and Eilers, J. (2005) Calbindin D28k Targets Myo-Inositol Monophosphatase in Spines and Dendrites of Cerebellar Purkinje Neurons. *Proc. Natl. Acad. Sci. U. S. A. 102* (16), 5850−5855.
(16) Blatow, M., Caputi, A., Burnashev, N., Monyer, H., and Rozov, A. (2003) Ca2+ Buffer Saturation Underlies Paired Pulse Facilitation in Calbindin-D28k-Containing Terminals. *Neuron 38* (1), 79−88.
(17) Müller, A., Kukley, M., Stausberg, P., Beck, H., Müller, W., and Dietrich, D. (2005) Endogenous Ca2+ Buffer Concentration and Ca2+ Microdomains in Hippocampal Neurons. *J. Neurosci. 25* (3), 558−565.
(18) Schmidt, H. (2012) Three Functional Facets of Calbindin D-28k. *Front. Mol. Neurosci. 5*, 25.
(19) Pan, P.-Y., and Ryan, T. A. (2012) Calbindin Controls Release Probability in Ventral Tegmental Area Dopamine Neurons. *Nat. Neurosci. 15*, 813.
(20) Brimblecombe, K. R., Gracie, C. J., Platt, N. J., and Cragg, S. J. (2015) Gating of Dopamine Transmission by Calcium and Axonal N, Q, T and L-Type Voltage-Gated Calcium Channels Differs between Striatal Domains. *J. Physiol. 593* (4), 929−946.
(21) Barski, J. J., Mörl, K., and Meyer, M. (2002) Conditional Inactivation of the Calbindin D-28k (Calb1) Gene by Cre/LoxP-Mediated Recombination. *Genesis 32* (2), 165−168.
(22) Bäckman, C. M., Malik, N., Zhang, Y., Shan, L., Grinberg, A., Hoffer, B. J., Westphal, H., and Tomac, A. C. (2006) Characterization of a Mouse Strain Expressing Cre Recombinase from the 3′ Untranslated Region of the Dopamine Transporter Locus. *Genesis 44* (8), 383−390.
(23) Wang, L., Zhang, X., Xu, H., Zhou, L., Jiao, R., Liu, W., Zhu, F., Kang, X., Liu, B., Teng, S., et al. (2014) Temporal Components of Cholinergic Terminal to Dopaminergic Terminal Transmission in Dorsal Striatum Slices of Mice. *J. Physiol. 592* (16), 3559−3576.
(24) Rice, M. E., and Cragg, S. J. (2004) Nicotine Amplifies Reward-Related Dopamine Signals in Striatum. *Nat. Neurosci. 7* (6), 583−584.
(25) Threlfell, S., Lalic, T., Platt, N. J., Jennings, K. A., Deisseroth, K., and Cragg, S. J. (2012) Striatal Dopamine Release Is Triggered by Synchronized Activity in Cholinergic Interneurons. *Neuron 75* (1), 58−64.
(26) Condon, M. D., Platt, N. J., Roberts, B. M., Tseu, M.-Y., Vietti-Michelina, S., Threlfell, S., and Cragg, S. J. (2018) Plasticity in Striatal Dopamine Release Is Governed by Release-Independent Depression and the Dopamine Transporter. *bioRxiv*, 392753.
(27) Schmidt, H., Kunerth, S., Wilms, C., Strotmann, R., and Eilers, J. (2007) Spino-Dendritic Cross-Talk in Rodent Purkinje Neurons Mediated by Endogenous Ca^{2+} -Binding Proteins. *J. Physiol. 581* (2), 619−629.
(28) Katz, B., and Miledi, R. (1968) The Role of Calcium in Neuromuscular Facilitation. *J. Physiol. 195* (2), 481−492.
(29) Ariel, P., Hoppa, M. B., and Ryan, T. A. (2013) Intrinsic Variability in Pv, RRP Size, Ca(2+) Channel Repertoire, and Presynaptic Potentiation in Individual Synaptic Boutons. *Front. Synaptic Neurosci. 4*, 9.
(30) Sakaba, T., and Neher, E. (2001) Quantitative Relationship between Transmitter Release and Calcium Current at the Calyx of Held Synapse. *J. Neurosci. 21* (2), 462−476.
(31) Stevens, C. F., and Wesseling, J. F. (1998) Activity-Dependent Modulation of the Rate at Which Synaptic Vesicles Become Available to Undergo Exocytosis. *Neuron 21* (2), 415−424.
(32) Wang, L.-Y., and Kaczmarek, L. K. (1998) High-Frequency Firing Helps Replenish the Readily Releasable Pool of Synaptic Vesicles. *Nature 394* (6691), 384−388.
(33) Schneggenburger, R., and Rosenmund, C. (2015) Molecular Mechanisms Governing Ca(2+) Regulation of Evoked and Spontaneous Release. *Nat. Neurosci. 18* (7), 935−941.
(34) Venton, B. J., Seipel, A. T., Phillips, P. E. M., Wetsel, W. C., Gitler, D., Greengard, P., Augustine, G. J., and Wightman, R. M. (2006) Cocaine Increases Dopamine Release by Mobilization of a Synapsin-Dependent Reserve Pool. *J. Neurosci. 26* (12), 3206−3209.
(35) Kile, B. M., Guillot, T. S., Venton, B. J., Wetsel, W. C., Augustine, G. J., and Wightman, R. M. (2010) Synapsins Differentially Control Dopamine and Serotonin Release. *J. Neurosci. 30* (29), 9762−9770.
(36) Ferris, M. J., España, R. A., Locke, J. L., Konstantopoulos, J. K., Rose, J. H., Chen, R., and Jones, S. R. (2014) Dopamine Transporters Govern Diurnal Variation in Extracellular Dopamine Tone. *Proc. Natl. Acad. Sci. U. S. A. 111* (26), E2751−9.
(37) John, C. E., and Jones, S. R. (2007) Voltammetric Characterization of the Effect of Monoamine Uptake Inhibitors and Releasers on Dopamine and Serotonin Uptake in Mouse Caudate-Putamen and Substantia Nigra Slices. *Neuropharmacology 52* (8), 1596−1605.
(38) Calipari, E. S., Huggins, K. N., Mathews, T. A., and Jones, S. R. (2012) Conserved Dorsal-Ventral Gradient of Dopamine Release and Uptake Rate in Mice, Rats and Rhesus Macaques. *Neurochem. Int. 61* (7), 986−991.
(39) Zhen, J., and Reith, M. E. A. (2018) Functional Properties of Dopamine Transporter Oligomers after Copper Linking. *J. Neurochem. 144* (2), 162−171.
(40) Gur, M., Cheng, M. H., Zomot, E., and Bahar, I. (2017) Effect of Dimerization on the Dynamics of Neurotransmitter:Sodium Symporters. *J. Phys. Chem. B 121* (15), 3657−3666.
(41) Chen, N., and Reith, M. E. A. (2008) Substrates Dissociate Dopamine Transporter Oligomers. *J. Neurochem. 105* (3), 910−920.
(42) Siciliano, C. A., Saha, K., Calipari, E. S., Fordahl, S. C., Chen, R., Khoshbouei, H., and Jones, S. R. (2018) Amphetamine Reverses Escalated Cocaine Intake via Restoration of Dopamine Transporter Conformation. *J. Neurosci. 38* (2), 484−497.
(43) Duda, J., Pötschke, C., and Liss, B. (2016) Converging Roles of Ion Channels, Calcium, Metabolic Stress, and Activity Pattern of *Substantia Nigra* Dopaminergic Neurons in Health and Parkinson's Disease. *J. Neurochem. 139*, 156−178.
(44) Miyazaki, I., and Asanuma, M. (2008) Dopaminergic Neuron-Specific Oxidative Stress Caused by Dopamine Itself. *Acta Med. Okayama 62* (3), 141−150.
(45) Airaksinen, M. S., Thoenen, H., and Meyer, M. (1997) Vulnerability of Midbrain Dopaminergic Neurons in Calbindin-D 28k -Deficient Mice: Lack of Evidence for a Neuroprotective Role of Endogenous Calbindin in MPTPtreated and Weaver Mice. *Eur. J. Neurosci. 9* (1), 120−127.
(46) Yuan, H.-H., Chen, R.-J., Zhu, Y.-H., Peng, C.-L., and Zhu, X.-R. (2013) The Neuroprotective Effect of Overexpression of Calbindin-D(28k) in an Animal Model of Parkinson's Disease. *Mol. Neurobiol. 47* (1), 117−122.
(47) Cragg, S. J., and Rice, M. E. (2004) DAncing Past the DAT at a DA Synapse. *Trends Neurosci. 27* (5), 270−277.
(48) Zhou, F. M., Liang, Y., and Dani, J. A. (2001) Endogenous Nicotinic Cholinergic Activity Regulates Dopamine Release in the Striatum. *Nat. Neurosci. 4* (12), 1224−1229.

DOI: 10.1021/acschemneuro.9b00325
ACS Chem. Neurosci. 2019, 10, 3419−3426